Li *et al. Genome Biology* (2025) 26:303
https://doi.org/10.1186/s13059-025-03801-5

Genome Biology

RESEARCH Open Access

Land plant-specific H3K27 methyltransferases ATXR5 and ATXR6 control plant development and stress responses

Xiaoyi Li[1,2,3†], Jie Pan[2,3†], Qian Liu[1], Huairen Zhang[2], Hui Li[2,3] and Danhua Jiang[1,2,3*]

†Xiaoyi Li and Jie Pan contributed equally to this work.

*Correspondence: danhua@tll.org.sg

[1] Temasek Life Sciences Laboratory, 1 Research Link, National University of Singapore, Singapore, Singapore
[2] State Key Laboratory of Seed Innovation, Institute of Genetics and Developmental Biology, Chinese Academy of Sciences, Beijing, China
[3] University of Chinese Academy of Sciences, Beijing, China

Abstract

Background: Histone modifications are critical for transcriptional regulation. A notable genetic innovation in land plants is the emergence of histone lysine methyltransferases ATXR5/6, which specifically catalyze the repressive histone H3 lysine 27 monomethylation (H3K27me1). Current knowledge of ATXR5/6 function is largely based on *Arabidopsis* studies using a weak *atxr5;atxr6* hypomorphic mutant, in which *ATXR6* is still partially expressed and defects are primarily observed in heterochromatin. However, the significance for land plants to evolve these enzymes remains unclear.

Results: In this study, we generate strong *atxr5;atxr6* mutants with further reduced *ATXR6* expression in *Arabidopsis* to explore the broader roles of ATXR5/6. Our results show that ATXR5/6 are essential for plant reproductive development and play a critical role in supporting normal plant growth by repressing the transcription of stress responsive genes. In addition, ATXR5/6 are necessary for maintaining H3K27 trimethylation (H3K27me3), likely by providing H3K27me1 as a substrate for further methylation. We also demonstrate that the function of ATXR5/6 in regulating development and responsive genes is conserved in the monocot rice.

Conclusions: Our findings suggest that land plants evolved ATXR5/6 not only to maintain heterochromatin, but also to regulate development and environmental responses, providing new insights into the functional significance of ATXR5/6 in land plants.

Background

In eukaryotes, epigenetic regulation, including post-translational modifications on histones, plays a pivotal role in determining the transcriptional activity [1]. Depending on their impact on transcription, histone modifications can either be "active" or "repressive." A well-studied repressive histone modification is histone H3 lysine 9 (H3K9) methylation, which serves as a conserved mark of heterochromatin across yeast, animals, and plants [2, 3]. In *Arabidopsis thaliana*, H3K9 methylation is primarily catalyzed by histone methyltransferases Su(var)3–9 homolog 4/Kryptonite (SUVH4/KYP), SUVH5, and

SUVH6 [4–7], and it predominantly silences the transcription of transposable elements (TEs) enriched at heterochromatin regions [5, 6, 8, 9].

Another repressive histone modification, the histone H3 lysine 27 trimethylation (H3K27me3), is primarily enriched at euchromatin regions and is associated with inactive protein-coding genes [10]. In animals, the enzymes responsible for catalyzing H3K27me3, namely the PRC2 complex, also deposit H3K27 monomethylation (H3K27me1) and H3K27 dimethylation (H3K27me2) [11, 12]. However, in land plants, two plant-specific H3K27me1 methyltransferases, ARABIDOPSIS TRITHORAX-RELATED PROTEIN 5 (ATXR5) and ATXR6, have evolved (Additional file 1: Fig. S1) [13, 14]. H3K27me1 is mainly found at heterochromatin regions in *Arabidopsis* [13, 15]. A weak *Arabidopsis atxr5;atxr6* double mutant exhibits decondensed heterochromatin, TE activation, and heterochromatin over-replication [13, 16]. Therefore, ATXR5/6-dependent H3K27me1 is regarded as a repressive histone modification that functions at heterochromatin in plants. However, the significance of land plants acquiring ATXR5/6 to deposit H3K27me1 remains unclear, especially given the presence of the already well-conserved heterochromatin mark H3K9 methylation. Although some genes at euchromatin are found to carry H3K27me1 in *Arabidopsis* [17, 18], this genic H3K27me1 may arise either from the activity of PRC2 or from the action of H3K27 demethylases, such as REF6, ELF6, and JMJ13, which can demethylate H3K27me3 to produce H3K27me1 [14, 17, 19, 20]. This hampers the efforts to identify the potential ATXR5/6-regulated genes through profiling H3K27me1 [17, 18]. Thus, it is of great interest to directly determine the biological importance of ATXR5/6.

In this study, we further investigate the functions of ATXR5/6 by generating strong *atxr5;atxr6* mutants in *Arabidopsis*. We show that ATXR5/6 are essential for both vegetative and reproductive development and are required to repress stress responsive genes. Moreover, we provide genome-wide evidence that ATXR5/6-mediated H3K27me1 is necessary for the maintenance of H3K27me3, thereby contributing to H3K27me3-mediated transcriptional repression. In addition, we demonstrate that ATXR5/6 perform conserved functions in rice. These findings suggest that ATXR5/6 help balance plant growth and stress responses beyond their role in heterochromatin maintenance, offering new insights into the significance of ATXR5/6 in land plants.

Results

Loss of *ATXR5* and *ATXR6* results in strong developmental defects

The so far commonly used *atxr5;atxr6* double mutant in *Arabidopsis* is a hypomorphic allele (referred to here as *atxr5;atxr6*^{hyp}), in which *ATXR6* is still expressed at moderate levels because a T-DNA was inserted at its promoter region. The *atxr5;atxr6*^{hyp} mutant displays only a slightly reduced growth phenotype compared with wild-type (WT) Columbia (Col) [13, 18]. To generate stronger mutants, we transformed CRISPR/Cas9 constructs targeting *ATXR6* into the *atxr5;atxr6*^{hyp} mutant and created deletions within the genic region of *ATXR6* (*atxr6*^{c}*-1* and *atxr6*^{c}*-2*), which result in premature termination of translation (Fig. 1a; Additional file 1: Fig. S2a). We failed to recover any *atxr6*^{c}*-1* or *atxr6*^{c}*-2* homozygotes from the progeny of *atxr5;atxr5;atxr6*^{hyp}*;atxr6*^{c}*-1* or *atxr5;atxr5;atxr6*^{hyp}*;atxr6*^{c}*-2* (Additional file 2: Table S1), indicating that null *atxr5;atxr6* mutants are lethal. Examination of seeds in

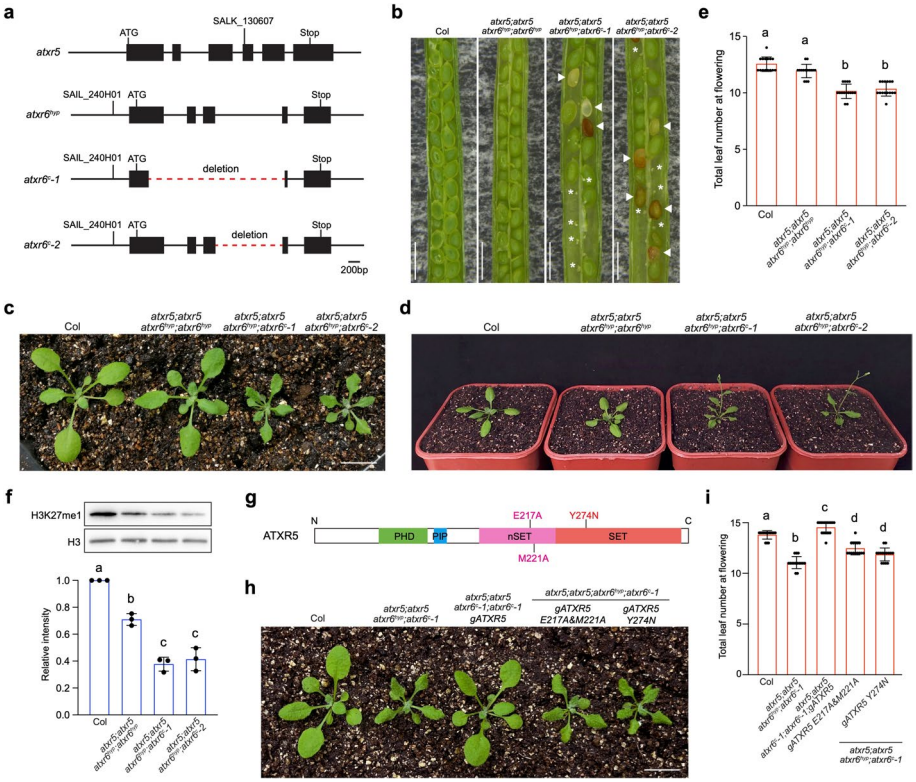

Fig. 1 ATXR5 and ATXR6 regulate plant development. **a** Schematic view of the full-length genomic structure of *ATXR5* and *ATXR6*. Filled boxes indicate exons, the red dashed lines represent deleted regions in *atxr6*^{c}*-1* and *atxr6*^{c}*-2*, and SALK_130637 and SAIL_240H01 are T-DNA insertions. **b** Seed developmental phenotypes of the indicated lines. Arrows indicate aborted seeds, while asterisks denote ovule-like structures. Scale bars, 1 mm. **c** Plant developmental phenotypes of the indicated lines. Scale bar, 1 cm. **d** Flowering phenotypes of the indicated lines. **e** Total number of primary rosette and cauline leaves at flowering for the indicated lines. Fifteen plants were scored for each line. Values are means ± SD. The significance of differences was tested using one-way ANOVA with Tukey's test ($P < 0.05$), with different letters indicating statistically significant differences. **f** H3K27me1 levels in the indicated lines determined by Western blotting. H3 was employed as a loading control. The bar chart represents the quantification of Western blot signals from three biological replicates (Additional file 1: Fig. S2c). Values are means ± SD. The significance of differences was tested using one-way ANOVA with Tukey's test ($P < 0.05$), with different letters indicating statistically significant differences. **g** Protein structure of ATXR5, the domains, and point mutations generated to deactivate ATXR5 are presented. **h** Plant developmental phenotypes of the complementation lines. Scale bar, 1 cm. **i** Total number of primary rosette and cauline leaves at flowering for the complementation lines. Fifteen plants were scored for each line. Values are means ± SD. The significance of differences was tested using one-way ANOVA with Tukey's test ($P < 0.05$), with different letters indicating statistically significant differences

the siliques of *atxr5;atxr5;atxr6*^{hyp}*;atxr6*^{c}*-1* and *atxr5;atxr5;atxr6*^{hyp}*;atxr6*^{c}*-2* revealed seed abortion during seed development (Fig. 1b). Moreover, small ovule-like structures were observed, which appeared to either not be fertilized or ceased development shortly after fertilization (Fig. 1b). Reciprocal crosses indicated that the loss of *ATXR5* and *ATXR6* severely impaired female gametogenesis, although transmission was still observed at low rates: less than 10% compared to the expected 50% (Additional file 2: Table S2). Hence, we conclude that *atxr5;atxr6*^{c}*-1* and *atxr5;atxr6*^{c}*-2* mutants are not viable due to female gametophytic and embryonic lethality. This finding is consistent with recent reports showing that the *atxr5;atxr6* null mutants are lethal [18, 21].

Although the *atxr5;atxr6* null mutants are not viable, we observed that *atxr5;atxr5;atxr6^{hyp};atxr6^{c}-1* and *atxr5;atxr5;atxr6^{hyp};atxr6^{c}-2* displayed stronger developmental defects, such as significantly smaller plants, compared to *atxr5;atxr6^{hyp}* at the vegetative stage (Fig. 1c). Moreover, they exhibited early flowering phenotypes (Fig. 1d, e). Examination of *ATXR6* expression revealed that its transcript levels were further reduced in *atxr5;atxr5;atxr6^{hyp};atxr6^{c}-1* and *atxr5;atxr5;atxr6^{hyp};atxr6^{c}-2* compared to *atxr5;atxr6^{hyp}* (Additional file 1: Fig. S2b), consistent with the more severe developmental defects observed in these mutants.

To determine whether ATXR5/6 regulate development via its enzymatic activity, we first analyzed global H3K27me1 levels in *atxr5;atxr5;atxr6^{hyp};atxr6^{c}-1* and *atxr5;atxr5;atxr6^{hyp};atxr6^{c}-2*. H3K27me1 levels were further diminished compared to *atxr5;atxr6^{hyp}* (Fig. 1f; Additional file 1: Fig. S2c), consistent with the more pronounced developmental defects. Next, we performed a complementation test with the full-length genomic *ATXR5* and the SET domain activity disrupted *ATXR5* (*gATXR5 E217A&M221A* and *gATXR5 Y274N*) (Fig. 1g) [16, 22]. Only WT *ATXR5* fully rescued the developmental defects (Fig. 1h, I; Additional file 1: Fig. S2d), suggesting that the enzymatic activity of ATXR5/6 is crucial for plant development.

The function of ATXR5/6 in plant developmental control seems different from that of H3K9 methyltransferases, as loss of SUVH4, SUVH5, and SUVH6 does not induce significant developmental abnormalities (Additional file 1: Fig. S3a) [23]. The *atxr5;atxr6^{hyp}* mutant bears excess DNA due to the over-replication of heterochromatin, particularly in endoreduplicated cells [16]. However, a comparable increase in DNA content was observed in *atxr5;atxr5;atxr6^{hyp};atxr6^{c}-1* and *atxr5;atxr5;atxr6^{hyp};atxr6^{c}-2* compared to *atxr5;atxr6^{hyp}* (Additional file 1: Fig. S3b, c), suggesting that the heterochromatin over-replication phenotype was not strongly enhanced in *atxr5;atxr5;atxr6^{hyp};atxr6^{c}-1* and *atxr5;atxr5;atxr6^{hyp};atxr6^{c}-2*. Moreover, similar percentages of nuclei in *atxr5;atxr6^{hyp}*, *atxr5;atxr5;atxr6^{hyp};atxr6^{c}-1* and *atxr5;atxr5;atxr6^{hyp};atxr6^{c}-2* showed decondensation of chromocenters enriched with heterochromatin (Additional file 1: Fig. S3d). These results suggest that the additional developmental defects observed in *atxr5;atxr5;atxr6^{hyp};atxr6^{c}-1* and *atxr5;atxr5;atxr6^{hyp};atxr6^{c}-2* compared to *atxr5;atxr6^{hyp}* are likely not due to heterochromatin misregulation. Since *atxr5;atxr5;atxr6^{hyp};atxr6^{c}-1* and *atxr5;atxr5;atxr6^{hyp};atxr6^{c}-2* exhibited similar phenotypes, we mainly used *atxr5;atxr5;atxr6^{hyp};atxr6^{c}-1* for subsequent studies.

Loss of *ATXR5* and *ATXR6* enhances plant resistance to bacterial infection

To explore potential reasons for the additional developmental abnormalities in *atxr5;atxr5;atxr6^{hyp};atxr6^{c}-1* compared to *atxr5;atxr6^{hyp}*, we compared their transcriptome changes. Hundreds of TEs and genes were significantly misexpressed in *atxr5;atxr6^{hyp}* and *atxr5;atxr5;atxr6^{hyp};atxr6^{c}-1* compared to WT Col (fold change > 2, *P*-adjust < 0.05), with the majority showing increased transcript levels (Fig. 2a; Additional file 2: Table S3, 4). This aligns with the notion that H3K27me1 is a repressive modification that inhibits transcription. *atxr5;atxr5;atxr6^{hyp};atxr6^{c}-1* and *atxr5;atxr6^{hyp}* had similar numbers of transcript level increased TEs, and nearly all of them were overlapped (Fig. 2a, b; Additional file 1: Fig. S4a). RT-qPCR validation of several overlapping TEs showed comparable activation levels in both genotypes (Additional file 1: Fig. S4b).

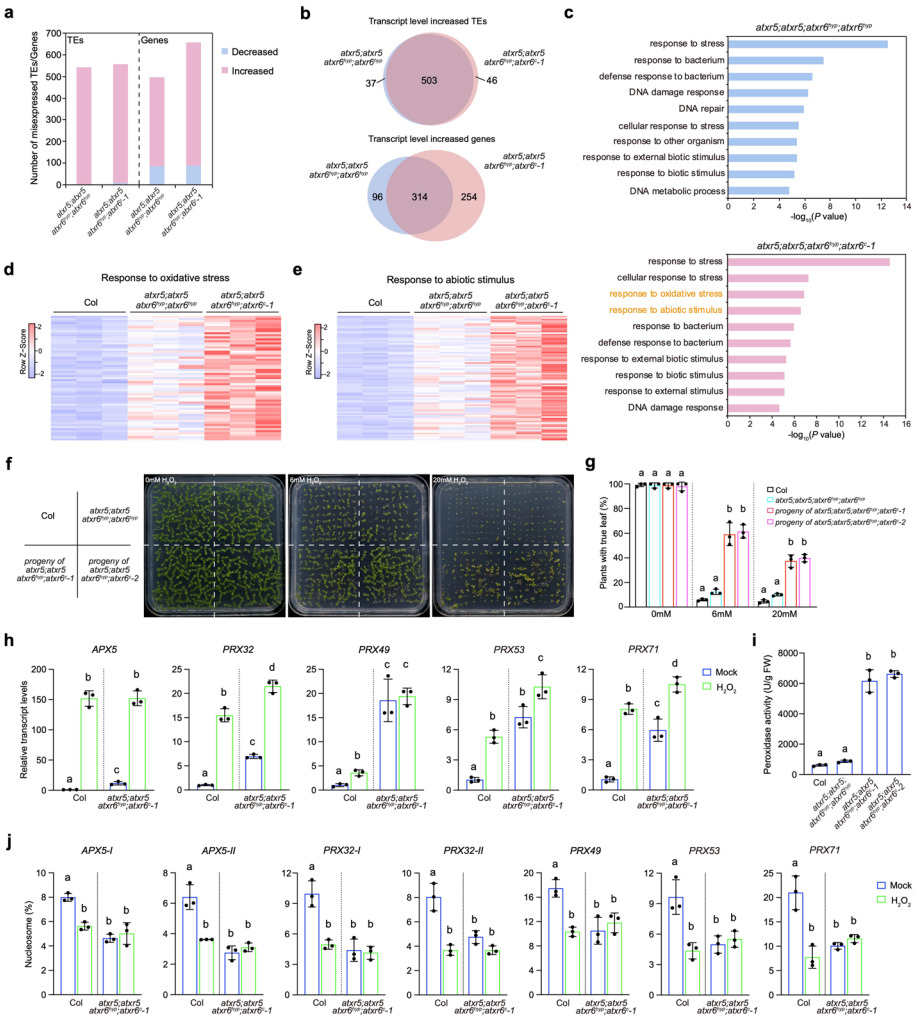

Fig. 2 Loss of ATXR5 and ATXR6 induces stress responses. **a** The number of significantly misexpressed TEs and genes in *atxr5;atxr6*^{hyp} and *atxr5;atxr5;atxr6*^{hyp}*;atxr6*^{c}*-1*. **b** Venn diagrams of transcript level significantly increased TEs and genes in *atxr5;atxr6*^{hyp} and *atxr5;atxr5;atxr6*^{hyp}*;atxr6*^{c}*-1*. **c** Gene ontology (GO) analysis on the transcript level significantly increased genes in *atxr5;atxr6*^{hyp} and *atxr5;atxr5;atxr6*^{hyp}*;atxr6*^{c}*-1*. Top 10 representative terms are listed and ranked by *P* value. GO terms specifically enriched in *atxr5;atxr5;atxr6*^{hyp}*;atxr6*^{c}*-1* are highlighted in orange font. **d** and **e** Heatmap showing transcript levels of oxidative stress response (d) and abiotic stimulus response (e) genes determined by RNA-seq. Results from three biological replicates are shown. **f** Seedling growth phenotypes on 1/2MS plate supplemented with either no H_2O_2 or with 6 mM or 20 mM H_2O_2. Pictures were taken 10 days after germination. **g** The true leaf formation rate of seedlings germinated on 1/2MS plate supplemented with either no H_2O_2 or with 6 mM or 20 mM H_2O_2. For the 0 mM and 6 mM H_2O_2 treatments, rates were measured 10 days after germination, while for the 20 mM H_2O_2 treatment, rate was measured 15 days after germination. Values are means ± SD of three biological replicates. At least 79 seeds were sown for each replicate. The significance of differences was tested using one-way ANOVA with Tukey's test ($P < 0.05$), with different letters indicating statistically significant differences. **h** Relative transcript levels of peroxidase-coding genes determined by RT-qPCR in Col and *atxr5;atxr5;atxr6*^{hyp}*;atxr6*^{c}*-1* with or without H_2O_2 treatment. Values are means ± SD of three biological replicates. The significance of differences was tested using one-way ANOVA with Tukey's test ($P < 0.05$), with different letters indicating statistically significant differences. **i** Peroxidase activity in the indicated lines. Values are means ± SD of three biological replicates. The significance of differences was tested using one-way ANOVA with Tukey's test ($P < 0.05$), with different letters indicating statistically significant differences. **j** H3K27me1 levels at peroxidase-coding genes determined by ChIP-qPCR in Col and *atxr5;atxr5;atxr6*^{hyp}*;atxr6*^{c}*-1* with or without H_2O_2 treatment. The amounts of immunoprecipitated DNA fragments were normalized to input DNA (mononucleosome). Values are means ± SD of three biological replicates. The significance of differences was tested using one-way ANOVA with Tukey's test ($P < 0.05$), with different letters indicating statistically significant differences

These results confirm our earlier observations that the *atxr5;atxr5;atxr6^{hyp};atxr6^{c}-1* and *atxr5;atxr5;atxr6^{hyp};atxr6^{c}-2* mutants did not show stronger defects at heterochromatin compared to *atxr5;atxr6^{hyp}* (Additional file 1: Fig. S3b–d). On the other hand, a substantial number of genes (254) were significantly activated only in *atxr5;atxr5;atxr6^{hyp};atxr6^{c}-1*, while a smaller set (96) was significantly activated only in *atxr5;atxr6^{hyp}* (Fig. 2b). Most of the genes and TEs that are identified to be significantly activated only in *atxr5;atxr6^{hyp}* also showed activation in *atxr5;atxr5;atxr6^{hyp};atxr6^{c}-1*, albeit at relatively lower levels (Additional file 1: Fig. S4c–e). It is possible that the further activation of these genes and TEs in *atxr5;atxr5;atxr6^{hyp};atxr6^{c}-1* might trigger an unknown feedback mechanism that diminishes their expression. Together, these results suggest that the further loss of H3K27me1 in *atxr5;atxr5;atxr6^{hyp};atxr6^{c}-1* mainly affects the repression of genes rather than TEs.

We further performed gene ontology (GO) analysis with transcript level significantly increased genes in *atxr5;atxr6^{hyp}* or *atxr5;atxr5;atxr6^{hyp};atxr6^{c}-1* to assess the functions of ATXR5/6-repressed genes. Both groups were found to be enriched in pathways related to response to bacteria and defense response (Fig. 2c; Additional file 1: Fig. S4f). In addition, the DNA damage response pathway was also enriched (Fig. 2c; Additional file 1: Fig. S4g), consistent with previous studies showing that DNA damage repair genes are activated in *atxr5;atxr6^{hyp}*, likely due to genome instability [18, 24]. We next tested whether the loss of ATXR5/6-induced activation of defense responsive genes affects plant resistance to the virulent bacterium *P. syringae* pathovar tomato (*Pst*) DC3000. Compared to WT, less severe disease symptoms were observed on the leaves of *atxr5;atxr6^{hyp}*, *atxr5;atxr5;atxr6^{hyp};atxr6^{c}-1*, and *atxr5;atxr5;atxr6^{hyp};atxr6^{c}-2* 3 days after inoculation of *Pst* DC3000 (Additional file 1: Fig. S5a). Consistently, bacterial growth was lower in these mutants compared to WT (Additional file 1: Fig. S5b). However, it is important to note that the activation of DNA damage responses could enhance plant immunity [25, 26]. Moreover, both *atxr5;atxr6^{hyp}* and *atxr5;atxr5;atxr6^{hyp};atxr6^{c}-1* showed similar increase in DNA damage and defense responses, suggesting that these activations do not account for the additional developmental defects observed in *atxr5;atxr5;atxr6^{hyp};atxr6^{c}-1* and *atxr5;atxr5;atxr6^{hyp};atxr6^{c}-2*.

ATXR5/6 repress plant oxidative stress response

Besides bacterial and DNA damage responses, GO analysis also revealed enrichment of oxidative stress and abiotic stimulus response pathways with transcript level significantly increased genes in *atxr5;atxr5;atxr6^{hyp};atxr6^{c}-1* but not in *atxr5;atxr6^{hyp}* (Fig. 2c–e), suggesting that the further loss of ATXR5/6 releases the repression of genes in these two pathways. To test whether loss of ATXR5/6 affects plant resistance to oxidative stress, seeds collected from WT Col, *atxr5;atxr6^{hyp}*, *atxr5;atxr5;atxr6^{hyp};atxr6^{c}-1*, and *atxr5;atxr5;atxr6^{hyp};atxr6^{c}-2* were germinated on 1/2MS plates containing hydrogen peroxide. Among the progeny of *atxr5;atxr5;atxr6^{hyp};atxr6^{c}-1* and *atxr5;atxr5;atxr6^{hyp};atxr6^{c}-2,* about half are expected to be *atxr5;atxr5;atxr6^{hyp};atxr6^{c}-1* or *atxr5;atxr5;atxr6^{hyp};atxr6^{c}-2*, respectively (Additional file 2: Table S1). By measuring the formation of true leaves, we found that the progeny of *atxr5;atxr5;atxr6^{hyp};atxr6^{c}-1* and *atxr5;atxr5;atxr6^{hyp};atxr6^{c}-2* exhibited greater resistance to hydrogen peroxide treatment compared to WT and the weak *atxr5;atxr6^{hyp}* mutant (Fig. 2f, g). Genotyping

analysis confirmed that most plants forming true leaves under hydrogen peroxide treatment were indeed *atxr5;atxr5;atxr6^{hyp};atxr6^{c}-1* or *atxr5;atxr5;atxr6^{hyp};atxr6^{c}-2*. Similarly, *atxr5;atxr5;atxr6^{hyp};atxr6^{c}-1* and *atxr5;atxr5;atxr6^{hyp};atxr6^{c}-2* displayed increased resistance to salt stress (Additional file 1: Fig. S6a, b), in agreement with the activation of abiotic stimulus response genes. The acquired resistance to oxidative and salt stresses in *atxr5;atxr5;atxr6^{hyp};atxr6^{c}-1* and *atxr5;atxr5;atxr6^{hyp};atxr6^{c}-2* is unlikely to result from activation of DNA damage responses, as DNA damage responses were also triggered in the non-resistant *atxr5;atxr6^{hyp}* mutant. Furthermore, treatment with genotoxic stress in WT Col did not strongly enhance resistance to oxidative and salt stresses (Additional file 1: Fig. S6c).

Notably, several peroxidase-coding genes were activated in *atxr5;atxr5;atxr6^{hyp};atxr6^{c}-1* compared to WT (Fig. 2d; Additional file 2: Table S3). Overexpression of peroxidase-coding genes has been reported to cause reduced plant growth, a phenotype similar to that observed in both *atxr5;atxr5;atxr6^{hyp};atxr6^{c}-1* and *atxr5;atxr5;atxr6^{hyp};atxr6^{c}-2* [27, 28]. In WT, the transcript levels of these peroxidase genes were induced by hydrogen peroxide treatment, suggesting that they are normally repressed in the absence of oxidative stress. However, their transcription was already activated in *atxr5;atxr5;atxr6^{hyp};atxr6^{c}-1*, and to a much lesser extent in *atxr5;atxr6^{hyp}*, even without stress (Fig. 2h; Additional file 1: Fig. S6d). Consistent with this, peroxidase activity was higher in *atxr5;atxr5;atxr6^{hyp};atxr6^{c}-1* and *atxr5;atxr5;atxr6^{hyp};atxr6^{c}-2* than in WT and *atxr5;atxr6^{hyp}* (Fig. 2i).

To examine whether ATXR5/6 repress the oxidative stress response through its enzymatic activity, we compared the oxidative stress response phenotypes of *atxr5;atxr5;atxr6^{hyp};atxr6^{c}-1* complemented with either WT or SET domain mutated ATXR5. Only the WT ATXR5, and not the SET domain mutated ones, restored susceptibility to oxidative stress (Additional file 1: Fig. S6e). Furthermore, enzymatic activity impaired ATXR5 was unable to repress the transcription of peroxidase-coding genes or reduce the peroxidase activity (Additional file 1: Fig. S6f, g). Thus, the repression of the oxidative stress response by ATXR5/6 is dependent on their enzymatic activity. We further analyzed H3K27me1 levels at these genes by ChIP-qPCR. H3K27me1 levels carried by these genes were reduced upon loss of ATXR5/6 (Fig. 2j; Additional file 1: Fig. S6h). Moreover, oxidative stress induced a decrease in H3K27me1 at these loci in WT (Fig. 2j). Together, these results suggest that the ATXR5/6-mediated H3K27me1 represses peroxidase-coding genes under normal growth conditions.

ATXR5/6 repress active histone modifications at peroxidase-coding genes

It was reported that ATXR5/6-mediated H3K27me1 antagonizes the deposition of active histone acetylation, such as H3K27 acetylation (H3K27ac) and H3K36ac, at the heterochromatin [29]. We speculate that H3K27me1 may also inhibit other active modifications. At this point, we selected H3K27ac and H3K36 trimethylation (H3K36me3) to examine their levels at peroxidase-coding genes in *atxr5;atxr5;atxr6^{hyp};atxr6^{c}-1*. Our results showed that H3K27ac and H3K36me3 levels were increased in *atxr5;atxr5;atxr6^{hyp};atxr6^{c}-1* compared to WT (Fig. 3a, b), suggesting that the ATXR5/6-mediated H3K27me1 represses their deposition at genes.

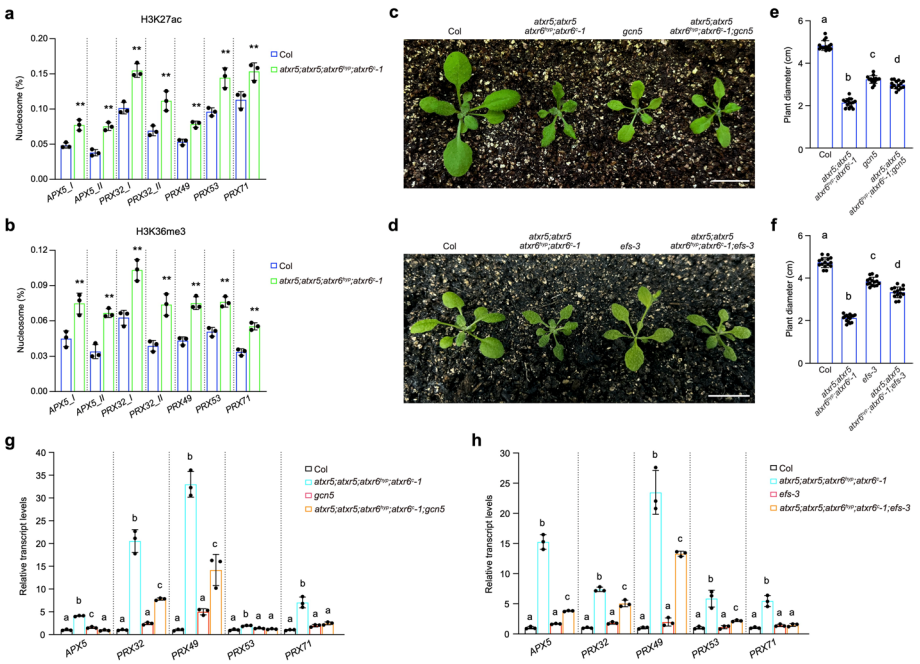

Fig. 3 ATXR5 and ATXR6 antagonize the accumulation of H3K27ac and H3K36me3 at peroxidase-coding genes. **a** and **b** H3K27ac (a) and H3K36me3 (b) levels at peroxidase-coding genes in Col and *atxr5;atxr5;atxr6*^{hyp}*;atxr6*^{c}*-1* determined by ChIP-qPCR. The amounts of immunoprecipitated DNA fragments were normalized to input DNA (mononucleosome). Values are means ± SD of three biological replicates. Statistical significance was determined by two-tailed Student's *t*-test (**, $P < 0.01$). **c** and **d** Plant developmental phenotypes following the loss of *GCN5* (c) or *EFS* (d) in *atxr5;atxr5;atxr6*^{hyp}*;atxr6*^{c}*-1*. Scale bars, 1 cm. **e** and **f** Plant diameters following the loss of *GCN5* (e) or *EFS* (f) in *atxr5;atxr5;atxr6*^{hyp}*;atxr6*^{c}*-1*. Fifteen 3-week-old plants were measured for each line. **g** and **h** Relative transcript levels of peroxidase-coding genes following the loss of GCN5 (g) or EFS (h) in *atxr5;atxr5;atxr6*^{hyp}*;atxr6*^{c}*-1* determined by RT-qPCR. Values are means ± SD of three biological replicates. The significance of differences was tested using one-way ANOVA with Tukey's test ($P < 0.05$), with different letters indicating statistically significant differences

We then crossed *atxr5;atxr5;atxr6*^{hyp}*;atxr6*^{c}*-1* with a mutant of GENERAL CONTROL NON-REPRESSED PROTEIN 5 (GCN5) or EARLY FLOWERING IN SHORT DAYS (EFS, also known as SDG8), which are histone acetylase and methyltransferase responsible for H3K27ac and H3K36me3 deposition, respectively [30, 31]. Although *gcn5* and *efs* mutants also exhibit developmental defects, they partially rescued the growth defects in *atxr5;atxr5;atxr6*^{hyp}*;atxr6*^{c}*-1*, as indicated by increased plant size (diameter) and improved leaf formation (Fig. 3c–f; Additional file 1: Fig. S7a, b). Furthermore, the absence of GCN5 or EFS in *atxr5;atxr5;atxr6*^{hyp}*;atxr6*^{c}*-1* partially inhibited the activation of peroxidase-coding genes and reduced the peroxidase activity (Fig. 3g, h; Additional file 1: Fig. S7c, d). Therefore, the H3K27me1 deposited by ATXR5/6 likely prevents the accumulation of active histone modifications, thereby inhibiting gene activation.

ATXR5/6 contribute to the maintenance of H3K27me3

The deposition of H3K27me1 by ATXR5/6 is considered replication coupled and primarily occurs on the replicative H3 variant H3.1 [22, 32]. Similarly, the maintenance of another repressive histone mark, H3K27me3, is also closely linked with DNA replication and depends on H3.1 [33–37]. It has been proposed that H3K27me1

deposition might facilitate the restoration of H3K27me3 after DNA replication [35, 38]. To assess the requirement of ATXR5/6 in H3K27me3 maintenance, we performed ChIP-seq to examine H3K27me3 profiles in WT and *atxr5;atxr5;atxr6*^{hyp}*;atxr6*^{c}*-1*. Interestingly, we observed a moderate reduction in H3K27me3 levels at H3K27me3-enriched regions in *atxr5;atxr5;atxr6*^{hyp}*;atxr6*^{c}*-1* compared with WT (Fig. 4a, b), and this reduction was consistently observed in both biological replicates performed (Additional file 1: Fig. S8a). Similarly, H3K27me3 levels were generally lower at H3K27me3-enriched genes in *atxr5;atxr5;atxr6*^{hyp}*;atxr6*^{c}*-1* (Additional file 1: Fig. S8b), with the majority of these genes showing a loss of H3K27me3 in *atxr5;atxr5;atxr6*^{hyp}*;atxr6*^{c}*-1* (Fig. 4c, d). This loss was accompanied by a moderate

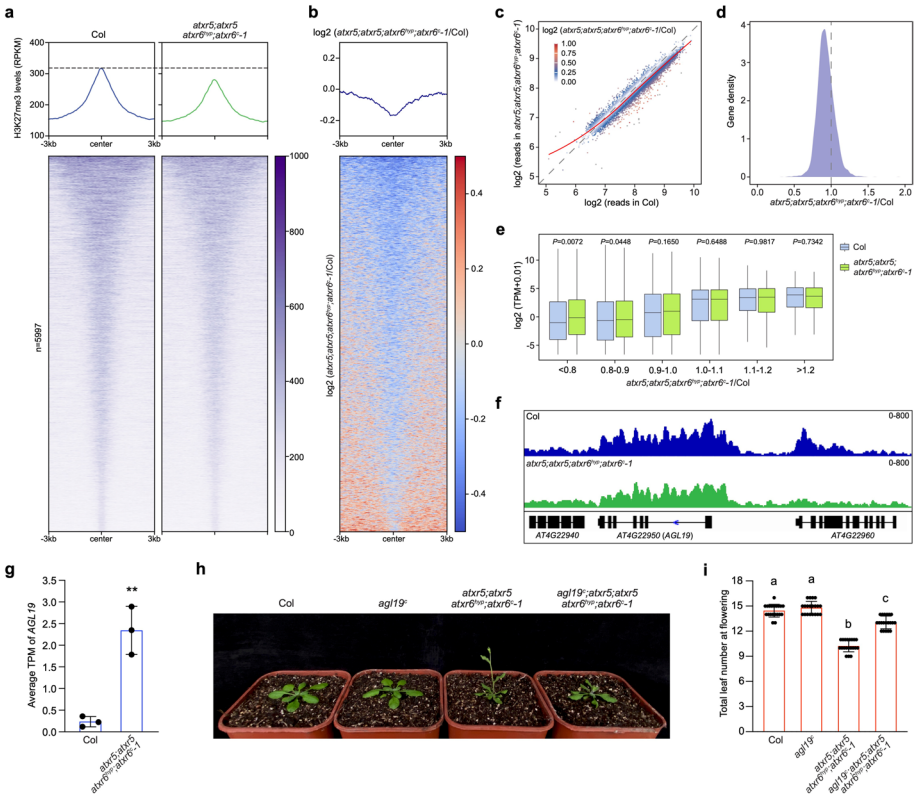

Fig. 4 ATXR5 and ATXR6 are required for the maintenance of H3K27me3. **a** Metaplots and heatmaps of H3K27me3 ChIP-seq signals in Col and *atxr5;atxr5;atxr6*^{hyp}*;atxr6*^{c}*-1* over H3K27me3-enriched peaks in WT Col. **b** Changes in H3K27me3 ChIP-seq signals in *atxr5;atxr5;atxr6*^{hyp}*;atxr6*^{c}*-1* compared to Col over H3K27me3-enriched peaks in WT Col. **c** Scatter plot showing H3K27m3 ChIP-seq reads in Col and *atxr5;atxr5;atxr6*^{hyp}*;atxr6*^{c}*-1* for all H3K27me3-enriched genes in WT Col. **d** Distribution of H3K27me3-enriched genes based on changes in H3K27me3 signals in *atxr5;atxr5;atxr6*^{hyp}*;atxr6*^{c}*-1* compared to Col. **e** Overall gene expression profiles of H3K27me3-enriched genes grouped according to changes in H3K27me3 levels in *atxr5;atxr5;atxr6*^{hyp}*;atxr6*^{c}*-1* compared to Col. The expression values represent the average of three biological replicates. *P* value is based on the Manne-Whitney *U* test. **f** Genome browser view of H3K27me3 accumulation levels at the locus encompassing *AGL19* in Col and *atxr5;atxr5;atxr6*^{hyp}*;atxr6*^{c}*-1*. **g** Average TPM values of *AGL19* in Col and *atxr5;atxr5;atxr6*^{hyp}*;atxr6*^{c}*-1* determined by RNA-seq. Values are means ± SD of three biological replicates. Statistical significance was determined by two-tailed Student's *t*-test (**, $P < 0.01$). **h** Flowering phenotypes following loss of *AGL19* in *atxr5;atxr5;atxr6*^{hyp}*;atxr6*^{c}*-1*. **i** Total number of primary rosette and cauline leaves at flowering for the indicated lines. Twenty plants were scored for each line. Values are means ± SD. The significance of differences was tested using one-way ANOVA with Tukey's test ($P < 0.05$), with different letters indicating statistically significant differences

increase in gene transcription, particularly for genes with a stronger reduction in H3K27me3 (Fig. 4e; Additional file 1: Fig. S8c). H3K27me3-enriched regions are predominantly marked by the replicative histone variant H3.1, rather than the non-replicative H3.3 (Additional file 1: Fig. S8d). Furthermore, genes with greater H3K27me3 loss in the *atxr5;atxr5;atxr6*^{hyp}*;atxr6*^{c}*-1* mutant tend to exhibit higher levels of both H3K27me3 and H3.1 in the wild type (Additional file 1: Fig. S8e). These observations are consistent with the preferential monomethylation of H3.1 at lysine 27 by ATXR5/6 [22]. The transcript levels of Polycomb group (PcG) genes, which regulate H3K27me3, as well as H3K27 demethylase-coding genes, were comparable between *atxr5;atxr5;atxr6*^{hyp}*;atxr6*^{c}*-1* and WT (Additional file 1: Fig. S8f). Hence, the reduction of H3K27me3 in *atxr5;atxr5;atxr6*^{hyp}*;atxr6*^{c}*-1* is not due to the misexpression of these genes.

Both the *atxr5;atxr5;atxr6*^{hyp}*;atxr6*^{c}*-1* and *atxr5;atxr5;atxr6*^{hyp}*;atxr6*^{c}*-2* displayed early flowering phenotypes (Fig. 1d, e). We noted that the floral activator *AGL19* and its upstream gene *AT4G22960*, which are both marked by H3K27me3, showed reduced H3K27me3 levels and increased transcript levels in *atxr5;atxr5;atxr6*^{hyp}*;atxr6*^{c}*-1* compared to WT (Fig. 4f, g; Additional file 1: Fig. S9a). In addition, the H3K27 monomethylation activity of ATXR5 is required for repressing both flowering and *AGL19* expression (Fig. 1i; Additional file 1: Fig. S9b). *AGL19* is strongly derepressed in PcG mutants, contributing to the early flowering phenotype in the loss of function mutant of CURLF LEAF (CLF), a key H3K27me3 methyltransferase in *Arabidopsis* [39]. To determine whether the early flowering phenotype of *atxr5;atxr5;atxr6*^{hyp}*;atxr6*^{c}*-1* is due to upregulated *AGL19* expression, we generated an *agl19* mutant (*agl19*^{c}) with CRISPR/Cas9 gene editing (Additional file 1: Fig. S9c, d) and introduced it into the *atxr5;atxr5;atxr6*^{hyp}*;atxr6*^{c}*-1* background. Loss of *AGL19* partially suppressed the early flowering phenotype (Fig. 4h, i), suggesting that ATXR5/6 repress flowering by assisting in the silencing of *AGL19*.

OsATXR5/6 regulate reproductive development and repress responsive genes in rice

ATXR5 and ATXR6 are conserved proteins across land plants. We thus further investigated their function in the monocot model plant rice (*Oryza sativa*) by knocking out their coding genes with CRISPR/Cas9 (Additional file 1: Fig. S10a–d). Similar to what we found in *Arabidopsis*, we were unable to recover the *osatxr5*^{c}*;osatxr6*^{c} double homozygous plants from the progeny of *osatxr5*^{c}*;osatxr6*^{c}*/+* (Additional file 2: Table S5). While *osatxr5*^{c}*;osatxr6*^{c}*/+* produced normal flower organs and pollen (Additional file 1: Fig. S10e, f), many empty grains were observed on the panicles, and its seed setting rate was lower than that of WT Nipponbare (NP) (Fig. 5a, b). The ratio of *osatxr5*^{c} to *osatxr5*^{c}*;osatxr6*^{c}*/+* in the progeny of *osatxr5*^{c}*;osatxr6*^{c}*/+* was approximately 1:2 (Additional file 2: Table S5). In addition, *osatxr5*^{c}*;osatxr6*^{c} mutations were successfully transmitted through both female and male gametes (Additional file 2: Table S6), suggesting that the *osatxr5*^{c}*;osatxr6*^{c} double homozygous is embryonic lethal. Thus, we conclude that OsATXR5/6 are essential for seed development but dispensable for gamete formation in rice.

The *osatxr5*^{c}*;osatxr6*^{c}*/+* mutant did not show obvious developmental defects at the vegetative stage (Fig. 5a). To assess the importance of OsATXR5/6 at this stage, we employed RNA interference (RNAi) strategy to knockdown Os*ATXR6*

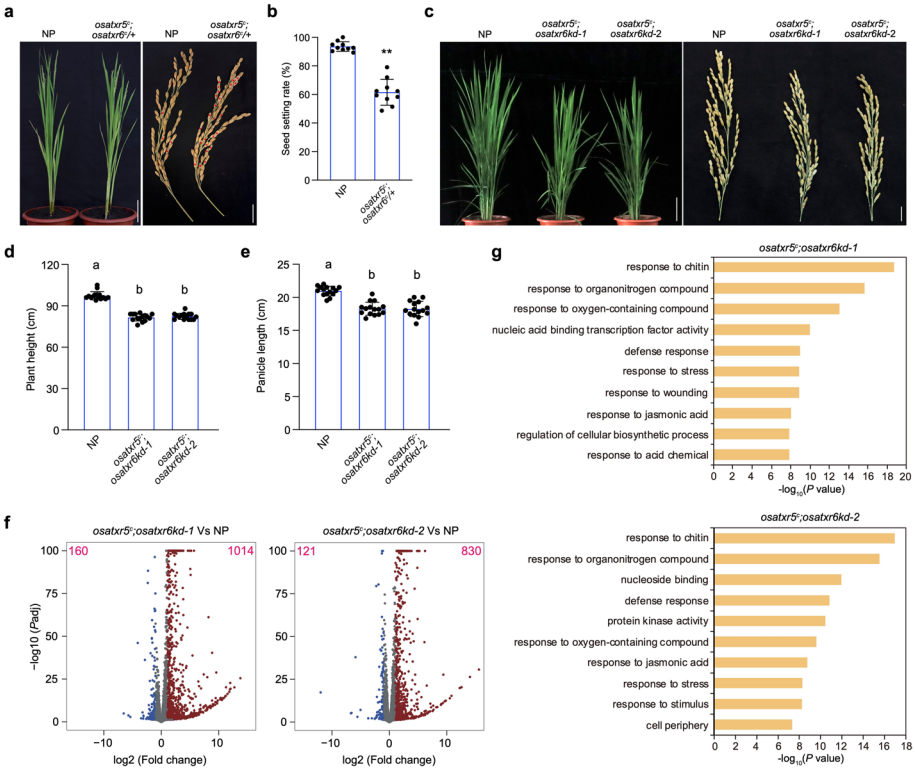

Fig. 5 OsATXR5/6 are essential for development and the repression of responsive genes in rice. **a** Plant (left) and panicle (right) phenotypes of NP and *osatxr5*^{c}*;osatxr6*^{c}*/+*. Empty grains are marked with red asterisks. Scale bars, 10 cm (left) and 2 cm (right). **b** Seed set rates on the panicles of NP and *osatxr5*^{c}*;osatxr6*^{c}*/+*. Ten panicles were counted for each line. Values are means ± SD. Statistical significance was determined by two-tailed Student's *t*-test (**, $P < 0.01$). **c** Plant (left) and panicle (right) phenotypes of NP, *osatxr5*^{c}*;osatxr6kd-1*, and *osatxr5*^{c}*;osatxr6kd-2*. Scale bars, 10 cm (left) and 2 cm (right). **d** and **e** Plant height (d) and panicle length (e) of NP, *osatxr5*^{c}*;osatxr6kd-1*, and *osatxr5*^{c}*;osatxr6kd-2*. Fifteen plants or panicles were scored for each line. Values are means ± SD. The significance of differences was tested using one-way ANOVA with Tukey's test ($P < 0.05$), with different letters indicating statistically significant differences. **f** Volcano plots of differentially expressed genes. The *y*-axis represents -log10 (*P* adjust), and the *x*-axis indicates log2 (fold change). Genes exhibiting at least a twofold change in expression and an adjusted *P* value of less than 0.05 are considered misexpressed. The numbers of genes with increased and decreased transcript levels are indicated in the top right and left corners, respectively. **g** Gene ontology (GO) analysis on transcript level significantly increased genes in *osatxr5*^{c}*;osatxr6kd-1* and *osatxr5*^{c}*;osatxr6kd-2*. Top 10 representative terms are listed and ranked by *P* value

expression (*osatxr6kd*) in the *osatxr5*^{c} mutant, and selected two independent lines for further studies (Additional file 1: Fig. S11a). Both lines exhibited decreased global H3K27me1 levels and displayed reduced growth phenotypes compared to NP (Fig. 5c–e; Additional file 1: Fig. S11b–f). We next performed RNA-seq with NP, *osatxr5*^{c}*;osatxr6kd-1*, and *osatxr5*^{c}*;osatxr6kd-2*. Hundreds of TEs and genes were misexpressed in *osatxr5*^{c}*;osatxr6kd-1* and *osatxr5*^{c}*;osatxr6kd-2*, with the majority being upregulated (Fig. 5f; Additional file 1: Fig. S11g; Additional file 2: Table S7, 8), further supporting the role of OsATXR5/6 in transcriptional repression. GO analysis revealed that the derepressed genes were primarily enriched in responsive pathways (Fig. 5g). Interestingly, DNA content analysis showed that the rice leaf predominantly contains 2C cells, and no extra DNA content was detected in *osatxr5*^{c}*;osatxr6kd-1*

and *osatxr5^{c};osatxr6kd-2* (Additional file 1: Fig. S11h, i). Moreover, DNA damage response genes were not activated in *osatxr5^{c};osatxr6kd-1* and *osatxr5^{c};osatxr6kd-2*, including those homologous to genes induced in the *Arabidopsis atxr5;atxr6* mutants (i.e., RAD51, BRCA1, GR1) (Fig. 5G; Additional file 1: Fig. S11j, k; Additional file 2: Table S7, 8) [24]. Thus, unlike in *Arabidopsis*, the loss of OsATXR5/6 causes transcriptional activation without compromising DNA stability in rice. Together, these results suggest that ATXR5/6 have conserved roles in regulating development and responsive genes in both *Arabidopsis* and rice.

Discussion

By generating strong *atxr5;atxr6* mutants in *Arabidopsis*, we have demonstrated that ATXR5/6 are crucial for regulating both plant development and abiotic stress responses. The function of ATXR5/6 in these processes relies on their enzymatic activity but is likely independent of their role in heterochromatin regulation, as the heterochromatin defects are comparable in the weak *atxr5;atxr6^{hyp}* and the strong *atxr5;atxr5;atxr6^{hyp};atxr6^{c}-1* and *atxr5;atxr5;atxr6^{hyp};atxr6^{c}-2* mutants, with only the latter two showing clear developmental abnormalities and enhanced resistance to abiotic stresses (Figs. 1 and 2; Additional file 1: Fig. S2–6). This aligns with the idea that heterochromatin defects in *Arabidopsis* per se do not typically cause strong developmental defects [40, 41]. On the other hand, the further loss of ATXR5/6 in the strong *atxr5;atxr6* mutant induces the derepression of many genes, including those responsive to oxidative stress and abiotic stimulus (Fig. 2a–e). ATXR5/6-mediated H3K27me1 is mainly enriched at heterochromatin regions [13, 17, 18]. It is possible that a partial loss of ATXR5/6 in the weak *atxr5;atxr6^{hyp}* mutant primarily impairs the deposition of H3K27me1 at heterochromatin, while a further loss of ATXR5/6 starts to cause defects at genic regions. This is further supported by the observations that complete loss of ATXR5/6 results in lethality, suggesting that a minimal level of ATXR5/6-mediated H3K27me1 is essential for plant viability.

Among the derepressed genes in the strong *atxr5;atxr6* mutant, there is a group of peroxidase-coding genes, including those encoding class III peroxidases (i.e., *PRX32*, *PRX49*, *PRX53*, *PRX71*). Class III peroxidases are plant-specific peroxidases that can reduce peroxide and oxidize a wide range of substrates, such as lignin precursor [42]. Only a few class III peroxidases are found in some streptopyhte algae, but they have been greatly expanded in land plants [42, 43]. Therefore, class III peroxidases may play a critical role by adapting the land plants to a more oxygenated environment and enabling the formation of rigid cell walls suitable for terrestrial life [42–44]. As antioxidants, peroxidases are also important for plant responses to environmental stresses, with many being induced by stress signals [45, 46]. However, overexpression of peroxidases leads to reduced plant growth [27, 28], suggesting that their expression must be tightly controlled. It is likely that ATXR5/6 repress peroxidase-coding genes under normal growth conditions to balance plant growth and stress response.

We found that a loss of H3K27me1 at peroxidase-coding genes is accompanied by an increase in H3K27ac and H3K36me3 (Fig. 2j; Fig. 3a, b), suggesting that H3K27me1 represses active histone modifications. Introducing GCN5 and EFS mutations into the *atxr5;atxr5;atxr6^{hyp};atxr6^{c}-1* mutant partially suppressed the activation

of peroxidase-coding genes (Fig. 3g, h). These observations are consistent with a recent study that reported an increase in H3K27ac at heterochromatin leading to heterochromatin defects and TE activation in *atxr5;atxr6*^{hyp} [29]. Therefore, AXTR5/6-mediated H3K27me1 appears to play a similar role in maintaining transcriptional silencing at both heterochromatin and genic regions by preventing the accumulation of active histone modifications.

In addition to depositing H3K27me1, we show that ATXR5/6 are also required for the maintenance of H3K27me3, a crucial histone modification in determining cellular identity (Fig. 4; Additional file 1: Fig. S8) [47]. This observation supports the previous hypothesis that the ATXR5/6-deposited H3K27me1 during DNA replication may serve as a substrate for the further catalyzation and rapid recovery of H3K27me3 after DNA replication in plants [35, 38]. Notably, H3K27me3 is only mildly affected in the strong *atxr5;atxr6* mutant. This may be due to the residual ATXR6 still providing some H3K27me1, or the H3K27me3 methyltransferases may be capable of synthesizing most H3K27me3 directly from unmethylated H3K27. Nevertheless, this mild loss of H3K27me3 leads to moderate depression of H3K27me3-enriched genes (Fig. 4e; Additional file 1: Fig. S8c), and, in particular, the flowering time regulatory gene *AGL19* becomes strongly activated upon loss of ATXR5/6, which contributes to the accelerated floral transition phenotype of the strong *atxr5;atxr6* mutant, suggesting the importance of the ATXR5/6-assisted H3K27me3 maintenance in controlling development and cellular identity. We propose that land plants may have evolved ATXR5/6 for the strict maintenance of H3K27me3, which is necessary to support their complex developmental programs and the great diversity of their cell types. Additional studies are needed to distinguish the effects of ATXR5/6-dependent H3K27me1 and H3K27me3 in plant development and stress responses.

To test the function of ATXR5/6 in other plants, we generated the null *osatxr5;osatxr6* mutant in rice and found that OsATXR5/6 are also essential for plant reproduction (Fig. 5a, b). However, unlike in *Arabidopsis*, OsATXR5/6 are required only for seed development and are dispensable for female gametogenesis. Further studies are needed to dissect the detailed functions of ATXR5/6 in plant reproductive development. In addition, by knocking down the expression of *OsATXR5/6*, we observed that the loss of OsATXR5/6 also leads to reduced plant growth and the depression of TEs and responsive genes (Fig. 5c–g; Additional file 1: Fig. S11c–g), suggesting the conserved function of OsATXR5/6 in repressing transcription and balancing plant growth and stress responses in rice. In *Arabidopsis*, the loss of ATXR5/6 results in genome instability, characterized by excess accumulation of heterochromatic DNA in endoreduplicated cells [16]. Interestingly, rice leaf cells lack endoreduplication, and no extra DNA was detected in the leaf nuclei of the *osatxr5;osatxr6* knockdown mutants (Additional file 1: Fig. S11h, i). This suggests that loss of ATXR5/6 induces transcriptional activation independent from affecting genome stability, at least in rice.

In conclusion, this study demonstrates that ATXR5/6 play conserved roles in controlling plant development and stress responses, which might be essential for terrestrial adaptation. This provides a possible explanation for the emergence of ATXR5/6 in land plants. Furthermore, our work highlights complex functions of ATXR5/6 in regulating transcriptional repression at both heterochromatin and genic regions through mediating

H3K27me1 and H3K27me3. Further studies are required to clarify these functions in more detail.

Conclusions

ATXR5 and ATXR6 are land plant-specific histone methyltransferases that catalyze H3K27me1, yet the significance of their acquisition in land plants remains unclear. In this study, we investigated the roles of ATXR5/6 in the dicot *Arabidopsis* and the monocot rice and found that they are essential for reproductive development. Specifically, ATXR5/6 are required for both female gametogenesis and embryogenesis in *Arabidopsis*, but only for embryogenesis in rice. In addition, our results demonstrate that ATXR5/6 are necessary for vegetative development in both species and function to repress the transcription of responsive genes, highlighting a conserved role in balancing growth and stress responses. Furthermore, we show that ATXR5/6 contribute to the global maintenance of H3K27me3 in *Arabidopsis*, likely by supplying H3K27me1 for further methylation, which is critical for the full repression of H3K27me3-marked genes. Together, these findings offer new insights into the functional significance of ATXR5/6 in land plants and lay the foundation for future studies on their land plant-specific evolution.

Methods

Plant materials and growth conditions

The *Arabidopsis atxr5;atxr6*^{hyp} [13], *gcn5* (Salk_150784) [48], and *efs-3* [49] have been previously described. *Arabidopsis* plants were grown under long day conditions (16-h light/8-h dark) at 22 °C. Rice plants were grown in paddy fields in Beijing, China.

Plasmid construction for plant transformation

CRISPR-Cas9 gene editing constructs containing two single-guide RNAs targeting *Arabidopsis ATXR6* or *AGL19* were generated using pHSE401 as previously described (Xing et al., 2014). Constructs for editing *OsATXR5* and *OsATXR6* were generated using pYLCRISPR/Cas9P$_{ubi}$-H, following the methods described by [50]. Guide RNA sequences are listed in Additional file 2: Table S9. All the mutations were confirmed via Sanger sequencing. For the complementation test, the genomic DNA of *ATXR5*, including its promoter, was inserted into the pHGW vector [51]. The *ATXR5* sequence was further mutated to generate *gATXR5 E217A&M221A* or *gATXR5 Y274N*. To knock down the expression of *OsATXR6* (*OsATXR6* RNAi), a 446 bp cDNA fragment, mainly from the 3′UTR region of *OsATXR6*, was PCR-amplified and cloned into the LH-FAD1390RNAi vector [52].

Measurement of plant diameter

Rosette diameter was measured as the distance from tip to tip of the longest rosette leaves in 3-week-old plants using ImageJ software. A total of 15 plants were measured for each line.

Pst DC3000 infection and bacteria number counting

Pst DC3000 infection was performed as previously described [53]. Briefly, *Pst* DC3000 was cultivated with KB medium containing rifampicin at 30 °C. After centrifugation, the

bacteria were resuspended in sterilized double distilled water (ddH2O) to an OD_{600} of 0.005. The bacterial suspension was infiltrated into *Arabidopsis* leaves using a syringe. Leaf discs with a 6-mm diameter were collected 3 h post-inoculation (0 DAI) or 3 days post-inoculation (3 DAI). The discs were washed with sterilized ddH_2O and ground in 100 μl of sterilized ddH2O. After adding 900 μl of sterilized ddH2O, the samples were thoroughly mixed and serially diluted 1:10. Then, 50 μl of each dilution was plated on TSA agar medium containing rifampicin, and colony numbers were counted after incubating at 30 °C for 2 days.

H2O2 and NaCl treatment

After-ripened seeds (harvested and stored at room temperature for at least 3 months) were sown on 1/2 MS medium, with or without H_2O_2 or NaCl. For the zeocin treatment, WT Col seeds were sown on 1/2 MS medium under the following conditions: without zeocin, with zeocin, without zeocin but with H_2O_2/NaCl, and with both zeocin and H_2O_2/NaCl. After stratification at 4 °C for 3 days, seeds were germinated under long-day conditions at 22 °C. Plants with true leaves were counted at 10, 14, or 15 days after germination. Two or three biological replicates were performed for each condition. For the H_2O_2 treatment in RT-qPCR and ChIP-qPCR experiments, 3-week-old *Arabidopsis* plants were sprayed with 20 mM H_2O_2 or with H_2O (as a mock control). Their leaves were collected 5 h after treatment.

Measurement of peroxidase activity

Peroxidase activity was measured using the peroxidase activity detection kit (Solarbio, BC0095) following the manufacturer's instruction. Briefly, 0.1 g of leaves from 3-week-old *Arabidopsis* plants was homogenized on ice using a mortar and pestle in 1-ml extraction buffer. After centrifugation, the supernatant was mixed with buffer 1, 2, and 3, and the absorbance was then measured with a spectrometer at OD_{470}.

Western blotting

Nuclei extracts from leaves of 3-week-old *Arabidopsis* plants or 40-day-old rice were separated by SDS-PAGE and then transferred to a 0.2-μm nitrocellulose membrane (GE Healthcare). Proteins were detected with anti-H3K27me1 (Millipore, 07–448) or anti-H3 (Abcam, ab1791) antibodies. The intensity of the protein bands were quantified using ImageJ and normalized to the H3 loading control.

DNA content analysis

For DNA content analysis, leaves from 3-week-old *Arabidopsis* plants and 40-day-old rice plants were chopped in Galbraith buffer (20 mM MOPS, 45 mM MgCl2, 30 mM sodium citrate, and 0.1% Triton X-100) for *Arabidopsis* or lysis buffer (25 mM Tris–HCl pH 7.6, 0.44 M sucrose, 10 mM MgCl2, 0.1% Triton X-100, 2 mM spermine, and 10 mM β-Mercaptoethanol) for rice. Then, samples were filtered through a 30-μm filter, and nuclei were stained with DAPI. Flow cytometry profiles were obtained using a BD FACSAria II cell sorter.

Pollen viability examination

Mature rice pollen grains were stained with a 1% I_2-KI solution and observed under a light microscope to assess viability.

Immunofluorescence

Immunostaining of isolated leaf nuclei was performed as previously described [36]. H3K27me1 signals were detected with anti-H3K27me1 antibody (Millipore, 07–448). Images were captured with a Zeiss confocal laser scanning microscope.

RNA-seq

For RNA-seq analysis, total RNA was extracted from leaves of 3-week-old *Arabidopsis* plants or 40-day-old rice plants using the Minibest plant RNA extraction kit (Takara, 9769), and three independent biological replicates were performed. Sequencing libraries were prepared with the NEBNext Ultra RNA library prep kit for Illumina (NEB, 7530L) according to the manufacturer's instruction. Prepared libraries were sequenced on a NovaSeq 6000 platform and paired-end 150 bp reads were generated. Adapter trimming was performed and low-quality reads were filtered with fastp version 0.20.1 [54]. Reads were aligned to the *Arabidopsis* genome (TAIR10) or the rice genome (RGAP, version 7.0) using Hisat2 version 2.1.10 [55]. Reads per gene were counted by HTseq version 0.11.2 [56]. Transcripts per million (TPM) values were generated using R. Differential gene expression analysis was performed using DESeq2 version 1.26.0 [57]. Genes were considered as differentially expressed if they exhibited a fold change greater than two and a *P* adjust value < 0.05. Gene ontology analysis was conducted with DAVID (https://david.ncifcrf.gov/) [58] for *Arabidopsis* and PlantRegMap (https://plantregmap.gao-lab.org/) [59] for rice.

ChIP-seq

ChIP-seq was performed using leaves from 3-week-old *Arabidopsis* plants, which were fixed with 1% formaldehyde. After nuclei extraction, mononucleosomes were generated by digesting with micrococcal nuclease (NEB, M0247S). Immunoprecipitation was conducted with anti-H3K27me3 antibody (Millipore, 07–449) as previously described [60]. Two independent biological replicates were performed. Immunoprecipitated DNA were subjected to library preparation with the VAHTS universal DNA library prep kit for Illumina (Vazyme, ND607-02) according to the manufacturer's instruction. Prepared libraries were sequenced on a NovaSeq 6000 platform and paired-end 150 bp reads were generated. Adapter trimming was performed and low-quality reads were filtered with fastp version 0.20.1 [54]. Reads were mapped to the *Arabidopsis* (TAIR10) genome with Bowtie2 version 2.4.2 [61]. Duplicate reads were filtered using Picard version 2.24.0 MarkDuplicates (https://github.com/broadinstitute/picard). H3K27me3 peaks in WT Col were called using MACS2 version 2.1.2 with input control and default parameters [62]. Only peaks identified in both biological replicates were retained. For data visualization, data from two biological replicates were merged, and bigwig coverage files were generated using deepTools

utility bamCoverage with a bin size of 10 bp [63]. Average ChIP-seq profiles were generated using deepTools utility plotProfile. For the analysis of H3.1 and H3.3 signals over H3K27me3-enriched peaks and genes, the H3.1 and H3.3 ChIP-seq data were obtained from a previous publication [64].

RT-qPCR

Total RNA was extracted from leaves of 3-week-old *Arabidopsis* plants or 1-week-old rice seedlings with Minibest plant RNA extraction kit (Takara, 9769), and three independent biological replicates were performed. Reverse transcription was performed using HiScript III 1st Strand cDNA Synthesis Kit (Vazyme, R312-02). Real-time quantitative PCR was conducted on an Applied Biosystems QuantStudio 6 Flex Real-Time PCR System using ChamQ Universal SYBR qPCR Master Mix (Vazyme, Q711-02). For normalization, *TUB2* was used as the endogenous control in *Arabidopsis*, and *OsUBQ5* was used in rice. Primers used for amplification are listed in Additional file 2: Table S10.

ChIP-qPCR

Leaves from 3-week-old *Arabidopsis* plants were fixed with 1% formaldehyde. After nuclei extraction, mononucleosomes were generated by digesting with micrococcal nuclease (NEB, M0247S). Immunoprecipitation was conducted with anti-H3K27me1 (Millipore, 07–448), anti-H3K27ac (Abclonal, a7253), or anti-H3K36me3 (Abcam, ab9050) antibody as previously described [60]. The amount of immunoprecipitated DNA was quantified by real-time PCR. Three independent biological replicates were performed. Primers used for amplification are listed in Additional file 2: Table S10.

Supplementary Information

The online version contains supplementary material available at https://doi.org/10.1186/s13059-025-03801-5.

Additional file 1: Supplementary figures. Figs. S1–S11.

Additional file 2: Supplementary tables. Tables S1–S10.

Additional file 3: Uncropped images for the blots in Fig. S2c.

Additional file 4: Uncropped images for the blots in Fig. S11b.

Acknowledgements
We thank Dr. Lei Li for the valuable advice on the bacterial infection experiment.

Peer review information
Wenjing She was the primary editor of this article and managed its editorial process and peer review in collaboration with the rest of the editorial team. The peer-review history is available in the online version of this article.

Authors' contributions
X.L., J.P., and D.J. designed experiments; X.L., J.P., H.L., and D.J. performed experiments; X.L., J.P., Q.L., and H.Z. analyzed data; D.J. wrote the paper with the help from X.L., J.P., and Q.L.; All authors read and approved the final manuscript.

Funding
This work was supported by the National Key R&D Program of China (2023YFD1200704) and the intramural research support from Temasek Life Sciences Laboratory.

Data availability
The RNA-seq datasets for Arabidopsis and rice, as well as the H3K27me3 ChIP-seq dataset for Arabidopsis generated in this study, are available in the NCBI Gene Expression Omnibus under accession numbers GSE278500 [65], GSE278501 [66], and GSE278502 [67], respectively. The H3.1 and H3.3 ChIP-seq datasets were obtained from a previous publication and are available under accession number GSE34840 [68].

Declarations

Ethics approval and consent to participate
Not applicable.

Consent for publication
Not applicable.

Competing interests
The authors declare no competing interests.

Received: 5 December 2024 Accepted: 17 September 2025
Published online: 25 September 2025

References

1. Zhao T, Zhan ZP, Jiang DH. Histone modifications and their regulatory roles in plant development and environmental memory. J Genet Genomics. 2019;46:467–76.
2. Montgomery SA, Tanizawa Y, Galik B, Wang N, Ito T, Mochizuki T, et al. Chromatin organization in early land plants reveals an ancestral association between H3K27me3, transposons, and constitutive heterochromatin. Curr Biol. 2020;30:573–88.
3. Naumann K, Fischer A, Hofmann I, Krauss V, Phalke S, Irmler K, et al. Pivotal role of AtSUVH2 in heterochromatic histone methylation and gene silencing in Arabidopsis. EMBO J. 2005;24:1418–29.
4. Du J, Johnson LM, Jacobsen SE, Patel DJ. DNA methylation pathways and their crosstalk with histone methylation. Nat Rev Mol Cell Biol. 2015;16:519–32.
5. Ebbs ML, Bartee L, Bender J. H3 lysine 9 methylation is maintained on a transcribed inverted repeat by combined action of SUVH6 and SUVH4 methyltransferases. Mol Cell Biol. 2005;25:10507–15.
6. Ebbs ML, Bender J. Locus-specific control of DNA methylation by the Arabidopsis SUVH5 histone methyltransferase. Plant Cell. 2006;18:1166–76.
7. Jackson JP, Lindroth AM, Cao X, Jacobsen SE. Control of CpNpG DNA methylation by the KRYPTONITE histone H3 methyltransferase. Nature. 2002;416:556–60.
8. Ding Y, Wang X, Su L, Zhai J, Cao S, Zhang D, et al. SDG714, a histone H3K9 methyltransferase, is involved in Tos17 DNA methylation and transposition in rice. Plant Cell. 2007;19:9–22.
9. Vaillant I, Paszkowski J. Role of histone and DNA methylation in gene regulation. Curr Opin Plant Biol. 2007;10:528–33.
10. Zhang X, Clarenz O, Cokus S, Bernatavichute YV, Pellegrini M, Goodrich J, et al. Whole-genome analysis of histone H3 lysine 27 trimethylation in Arabidopsis. PLoS Biol. 2007;5:e129.
11. Ebert A, Schotta G, Lein S, Kubicek S, Krauss V, Jenuwein T, et al. Su(var) genes regulate the balance between euchromatin and heterochromatin in *Drosophila*. Genes Dev. 2004;18:2973–83.
12. Shen X, Liu Y, Hsu YJ, Fujiwara Y, Kim J, Mao X, et al. EZH1 mediates methylation on histone H3 lysine 27 and complements EZH2 in maintaining stem cell identity and executing pluripotency. Mol Cell. 2008;32:491–502.
13. Jacob Y, Feng S, LeBlanc CA, Bernatavichute YV, Stroud H, Cokus S, et al. ATXR5 and ATXR6 are H3K27 monomethyltransferases required for chromatin structure and gene silencing. Nat Struct Mol Biol. 2009;16:763–8.
14. Jacob Y, Michaels SD. H3K27me1 is E(z) in animals, but not in plants. Epigenetics. 2009;4:366–9.
15. Mathieu O, Probst AV, Paszkowski J. Distinct regulation of histone H3 methylation at lysines 27 and 9 by CpG methylation in Arabidopsis. EMBO J. 2005;24:2783–91.
16. Jacob Y, Stroud H, Leblanc C, Feng S, Zhuo L, Caro E, et al. Regulation of heterochromatic DNA replication by histone H3 lysine 27 methyltransferases. Nature. 2010;466:987–91.
17. Antunez-Sanchez J, Naish M, Ramirez-Prado JS, Ohno S, Huang Y, Dawson A, Opassathian K, Manza-Mianza D, Ariel F, Raynaud C, et al. A new role for histone demethylases in the maintenance of plant genome integrity. Elife. 2020;9:e58533.
18. Potok ME, Zhong Z, Picard CL, Liu Q, Do T, Jacobsen CE, Sakr O, Naranbaatar B, Thilakaratne R, Khnkoyan Z, et al. The role of ATXR6 expression in modulating genome stability and transposable element repression in Arabidopsis. Proc Natl Acad Sci U S A. 2022;119:e2115570119.
19. Lu F, Cui X, Zhang S, Jenuwein T, Cao X. *Arabidopsis* REF6 is a histone H3 lysine 27 demethylase. Nat Genet. 2011;43:715–9.
20. Zheng S, Hu H, Ren H, Yang Z, Qiu Q, Qi W, et al. The Arabidopsis H3K27me3 demethylase JUMONJI 13 is a temperature and photoperiod dependent flowering repressor. Nat Commun. 2019;10:1303.
21. Zhao X, Wang J, Jin D, Cheng J, Chen H, Li Z, et al. AtMCM10 promotes DNA replication-coupled nucleosome assembly in Arabidopsis. J Integr Plant Biol. 2023;65:203–22.
22. Jacob Y, Bergamin E, Donoghue MT, Mongeon V, LeBlanc C, Voigt P, et al. Selective methylation of histone H3 variant H3.1 regulates heterochromatin replication. Science. 2014;343:1249–53.
23. Yu CW, Tai R, Wang SC, Yang P, Luo M, Yang S, et al. Histone deacetylase6 acts in concert with histone methyltransferases SUVH4, SUVH5, and SUVH6 to regulate transposon silencing. Plant Cell. 2017;29:1970–83.
24. Stroud H, Hale CJ, Feng S, Caro E, Jacob Y, Michaels SD, et al. DNA methyltransferases are required to induce heterochromatic re-replication in Arabidopsis. PLoS Genet. 2012;8:e1002808.
25. Wang S, Durrant WE, Song J, Spivey NW, Dong X. *Arabidopsis* BRCA2 and RAD51 proteins are specifically involved in defense gene transcription during plant immune responses. Proc Natl Acad Sci USA. 2010;107:22716–21.
26. Yan S, Wang W, Marqués J, Mohan R, Saleh A, Durrant Wendy E, et al. Salicylic acid activates DNA damage responses to potentiate plant immunity. Mol Cell. 2013;52:602–10.

27. Pedreira J, Herrera MT, Zarra I, Revilla G. The overexpression of AtPrx37, an apoplastic peroxidase, reduces growth in Arabidopsis. Physiol Plant. 2011;141:177–87.
28. Raggi S, Ferrarini A, Delledonne M, Dunand C, Ranocha P, De Lorenzo G, et al. The Arabidopsis class III peroxidase AtPRX71 negatively regulates growth under physiological conditions and in response to cell wall damage. Plant Physiol. 2015;169:2513–25.
29. Dong J, LeBlanc C, Poulet A, Mermaz B, Villarino G, Webb KM, et al. H3.1K27me1 maintains transcriptional silencing and genome stability by preventing GCN5-mediated histone acetylation. Plant Cell. 2021;33:961–79.
30. Chen C, Li C, Wang Y, Renaud J, Tian G, Kambhampati S, et al. Cytosolic acetyl-CoA promotes histone acetylation predominantly at H3K27 in Arabidopsis. Nat Plants. 2017;3:814–24.
31. Xu L, Zhao Z, Dong A, Soubigou-Taconnat L, Renou JP, Steinmetz A, et al. Di- and tri- but not monomethylation on histone H3 lysine 36 marks active transcription of genes involved in flowering time regulation and other processes in *Arabidopsis thaliana*. Mol Cell Biol. 2008;28:1348–60.
32. Raynaud C, Sozzani R, Glab N, Domenichini S, Perennes C, Cella R, et al. Two cell-cycle regulated SET-domain proteins interact with proliferating cell nuclear antigen (PCNA) in Arabidopsis. Plant J. 2006;47:395–407.
33. Del Olmo I, Lopez JA, Vazquez J, Raynaud C, Pineiro M, Jarillo JA. *Arabidopsis* DNA polymerase recruits components of Polycomb repressor complex to mediate epigenetic gene silencing. Nucleic Acids Res. 2016;44:5597–614.
34. Hyun Y, Yun H, Park K, Ohr H, Lee O, Kim DH, et al. The catalytic subunit of Arabidopsis DNA polymerase alpha ensures stable maintenance of histone modification. Development. 2013;140:156–66.
35. Jiang D, Berger F. DNA replication-coupled histone modification maintains polycomb gene silencing in plants. Science. 2017;357:1146–9.
36. Wang L, Xue M, Zhang H, Ma L, Jiang D. TONSOKU is required for the maintenance of repressive chromatin modifications in Arabidopsis. Cell Rep. 2023;42:112738.
37. Zhou Y, Tergemina E, Cui H, Forderer A, Hartwig B, Velikkakam James G, et al. Ctf4-related protein recruits LHP1-PRC2 to maintain H3K27me3 levels in dividing cells in Arabidopsis thaliana. Proc Natl Acad Sci U S A. 2017;114:4833–8.
38. Borg M, Jiang D, Berger F. Histone variants take center stage in shaping the epigenome. Curr Opin Plant Biol. 2021;61:101991.
39. Schonrock N, Bouveret R, Leroy O, Borghi L, Kohler C, Gruissem W, et al. Polycomb-group proteins repress the floral activator AGL19 in the FLC-independent vernalization pathway. Genes Dev. 2006;20:1667–78.
40. Vongs A, Kakutani T, Martienssen RA, Richards EJ. *Arabidopsis thaliana* DNA methylation mutants. Science. 1993;260:1926–8.
41. Bourguet P, Picard CL, Yelagandula R, Pélissier T, Lorković ZJ, Feng S, et al. The histone variant H2A.W and linker histone H1 co-regulate heterochromatin accessibility and DNA methylation. Nat Commun. 2021;12:2683.
42. Passardi F, Longet D, Penel C, Dunand C. The class III peroxidase multigenic family in rice and its evolution in land plants. Phytochemistry. 2004;65:1879–93.
43. Mbadinga Mbadinga DL, Li Q, Ranocha P, Martinez Y, Dunand C. Global analysis of non-animal peroxidases provides insights into the evolution of this gene family in the green lineage. J Exp Bot. 2020;71:3350–60.
44. Passardi F, Bakalovic N, Teixeira FK, Margis-Pinheiro M, Penel C, Dunand C. Prokaryotic origins of the non-animal peroxidase superfamily and organelle-mediated transmission to eukaryotes. Genomics. 2007;89:567–79.
45. Eljebbawi A, Savelli B, Libourel C, Estevez JM, Dunand C. Class III peroxidases in response to multiple abiotic stresses in Arabidopsis thaliana Pyrenean populations. Int J Mol Sci. 2022;23:3960.
46. Kidwai M, Ahmad IZ, Chakrabarty D. Class III peroxidase: an indispensable enzyme for biotic/abiotic stress tolerance and a potent candidate for crop improvement. Plant Cell Rep. 2020;39:1381–93.
47. Wiles ET, Selker EU. H3K27 methylation: a promiscuous repressive chromatin mark. Curr Opin Genet Dev. 2017;43:31–7.
48. Kornet N, Scheres B. Members of the GCN5 histone acetyltransferase complex regulate PLETHORA-mediated root stem cell niche maintenance and transit amplifying cell proliferation in Arabidopsis. Plant Cell. 2009;21:1070–9.
49. Kim SY, He YH, Jacob Y, Noh YS, Michaels S, Amasino R. Establishment of the vernalization-responsive, winter-annual habit in *Arabidopsis* requires a putative histone H3 methyl transferase. Plant Cell. 2005;17:3301–10.
50. Ma X, Zhang Q, Zhu Q, Liu W, Chen Y, Qiu R, et al. A robust CRISPR/Cas9 system for convenient, high-efficiency multiplex genome editing in monocot and dicot plants. Mol Plant. 2015;8:1274–84.
51. Karimi M, Inze D, Depicker A. Gateway vectors for Agrobacterium-mediated plant transformation. Trends Plant Sci. 2002;7:193–5.
52. Zhang BQ, Liu XS, Feng SJ, Zhao YN, Wang LL, Rono JK, et al. Developing a cadmium resistant rice genotype with OsHIPP29 locus for limiting cadmium accumulation in the paddy crop. Chemosphere. 2020;247:125958.
53. Yamaguchi Y, Huffaker A, Bryan AC, Tax FE, Ryan CA. PEPR2 is a second receptor for the Pep1 and Pep2 peptides and contributes to defense responses in Arabidopsis. Plant Cell. 2010;22:508–22.
54. Chen SF, Zhou YQ, Chen YR, Gu J. Fastp: an ultra-fast all-in-one FASTQ preprocessor. Bioinformatics. 2018;34:884–90.
55. Kim D, Paggi JM, Park C, Bennett C, Salzberg SL. Graph-based genome alignment and genotyping with HISAT2 and HISAT-genotype. Nat Biotechnol. 2019;37:907.
56. Anders S, Pyl PT, Huber W. HTSeq-a python framework to work with high-throughput sequencing data. Bioinformatics. 2015;31:166–9.
57. Love MI, Huber W, Anders S. Moderated estimation of fold change and dispersion for RNA-seq data with DESeq2. Genome Biol. 2014;15:550.
58. Huang DW, Sherman BT, Lempicki RA. Systematic and integrative analysis of large gene lists using DAVID bioinformatics resources. Nat Protoc. 2009;4:44–57.
59. Tian F, Yang D-C, Meng Y-Q, Jin J, Gao G. Plantregmap: charting functional regulatory maps in plants. Nucleic Acids Res. 2019;48:D1104–13.
60. Pan J, Zhang H, Zhan Z, Zhao T, Jiang D. A REF6-dependent H3K27me3-depleted state facilitates gene activation during germination in Arabidopsis. J Genet Genomics. 2023;50:178–91.
61. Langmead B, Salzberg SL. Fast gapped-read alignment with Bowtie 2. Nat Methods. 2012;9:357–59.

62. Zhang Y, Liu T, Meyer CA, Eeckhoute J, Johnson DS, Bernstein BE, et al. Model-based analysis of ChIP-Seq (MACS). Genome Biol. 2008;9:R137.
63. Ramirez F, Dundar F, Diehl S, Gruning BA, Manke T. deepTools: a flexible platform for exploring deep-sequencing data. Nucleic Acids Res. 2014;42:W187–91.
64. Stroud H, Otero S, Desvoyes B, Ramirez-Parra E, Jacobsen SE, Gutierrez C. Genome-wide analysis of histone H3.1 and H3.3 variants in *Arabidopsis thaliana*. Proc Natl Acad Sci U S A. 2012;109:5370–5.
65. Li X, Pan J, Liu Q, Zhang H, Li H, Jiang D. Land plant-specific H3K27 methyltransferases ATXR5 and ATXR6 control plant development and stress responses. Datasets. NCBI Gene Expression Omnibus. 2024. https://www.ncbi.nlm.nih.gov/geo/query/acc.cgi?acc=GSE278500.
66. Li X, Pan J, Liu Q, Zhang H, Li H, Jiang D. Land plant-specific H3K27 methyltransferases ATXR5 and ATXR6 control plant development and stress responses. Datasets. NCBI Gene Expression Omnibus. 2024. https://www.ncbi.nlm.nih.gov/geo/query/acc.cgi?acc=GSE278501.
67. Li X, Pan J, Liu Q, Zhang H, Li H, Jiang D. Land plant-specific H3K27 methyltransferases ATXR5 and ATXR6 control plant development and stress responses. Datasets. NCBI Gene Expression Omnibus. 2024. https://www.ncbi.nlm.nih.gov/geo/query/acc.cgi?acc=GSE278502.
68. Otero S, Desvoyes B, Ramirez-Parra E, Jacobsen SE, Gutierrez C. Genome-wide analysis of histone H3.1 and H3.3 variants in Arabidopsis thaliana. Datasets. NCBI Gene Expression Omnibus. 2012. https://www.ncbi.nlm.nih.gov/geo/query/acc.cgi?acc=GSE34840.

Publisher's Note